Cellular Signalling 55 (2019) 40–52

Contents lists available at ScienceDirect

Cellular Signalling

journal homepage: www.elsevier.com/locate/cellsig

A potential regulatory network among WDR86-AS1, miR-10b-3p, and LITAF is possibly involved in preeclampsia pathogenesis

Ruizhen Li, Nan Wang, Min Xue*, Wenxin Long, Chunxia Cheng, Chunmei Mi, Zhou Gao

Department of Obstetrics and Gynecology, The Third Xiangya Hospital of Central South University, Changsha, Hunan 410013, PR China

ARTICLE INFO

Keywords:
WDR86-AS1
miR-10b-3p
LITAF
Preeclampsia pathogenesis

ABSTRACT

Preeclampsia (PE), a pregnancy-specific disorder, is a leading cause of perinatal maternal and fetal mortality and morbidity. Impaired migration and invasion of trophoblastic cells and an imbalanced systemic maternal inflammatory response have been proposed as possible causes of pathogenesis of PE. Comparative analysis of PE-affected placentas and healthy placentas has uncovered differentially expressed long noncoding RNAs, microRNAs, and mRNAs. This study was conducted to investigate the effect of a regulatory network among these RNAs on PE pathogenesis. Long noncoding RNA WDR86-AS1, microRNA miR-10b-3p, and mRNA of protein LITAF were identified by screening of genes in existing databases with aberrant expression in PE-affected placentas and potential mutual interactions as revealed by TargetScan, miRanda, and PicTar analyses. This study identified their expression in PE-affected and healthy placentas by RT-PCR. An *in vitro* experiment was performed on human trophoblast HTR-8/SVneo cells cultured under normoxic or hypoxic conditions. MiR-10b-3p targets were identified in luciferase reporter assays and RNA pull-down assays. The mouse model of PE was set up using a soluble form of FLT-1 for *in vivo* testing. Lower levels of miR-10b-3p but higher expression of WDR86-AS1 and LITAF were observed in PE-affected placentas and trophoblast cells under hypoxia. WDR86-AS1 and *LITAF* mRNA were confirmed as targets of miR-10b-3p. WDR86-AS1 downregulated miR-10b-3p but promoted LITAF expression. Microarray analyses revealed that LITAF controlled the inflammatory responses and migration and proliferation of HTR-8/SVneo cells under hypoxia. Indeed, knockdown of WDR86-AS1 and LITAF or overexpression of miR-10b-3p attenuated the hypoxia-induced inhibition of cellular viability, migration, and invasion. Moreover, miR-10b-3p overexpression attenuated the pathological symptoms caused by soluble FLT-1 *in vivo*. In summary, the WDR86-AS1/miR-10b-3p/LITAF network is probably involved in PE pathogenesis.

1. Introduction

Preeclampsia (PE), affecting 5–8% of all pregnancies, remains one of the leading causes of maternal and fetal morbidity and mortality worldwide [1,2]. Patients with PE show severe maternal hypertension and proteinuria, commonly after the 20th week of gestation, and no effective therapy is currently available except for a timed and often preterm delivery [1,2]. It has been widely acknowledged that defects in placental development during the early stages of pregnancy are the main risk factors of PE, although the molecular mechanisms underlying the aberrant placental development are not fully understood [3]. The placenta is a highly specialized organ responsible for the delivery of oxygen and nutrients to the developing fetus. The development of placenta involves the invasion of trophoblastic cells from chorionic villi into the inner third of the myometrium and into the spiral arteries in the uterine wall for spiral artery remodeling. Nonetheless, in PE, the trophoblast invasion of the myometrium is frequently shallow, causing incomplete spiral artery remodeling. The impaired spiral artery remodeling is associated with aberrant placental perfusion, with local hypoxia, and oxidative stress [3]. Under these pathological conditions, villous trophoblasts release proinflammatory cytokines into the placenta and maternal circulation, thereby causing placental and systemic inflammation. The inflammation not only impairs the function of the placenta but also causes endothelial dysfunction that results in maternal clinical symptoms [3,4].

Lipopolysaccharide (LPS)-induced tumor necrosis factor α factor (LITAF), alternatively known as small integral membrane protein of the lysosome/late endosome (SIMPLE) and as p53-inducible gene 7 (PIG-7) protein, has been identified as an important player in the activation of proinflammatory molecules. The *LITAF* gene has been mapped to chromosomal region 16p12–16p13.3 in humans [5]. It encodes a transcription factor that can bind to a CTCCC (positions −515 to

* Corresponding author.
E-mail address: minxue985@163.com (M. Xue).

https://doi.org/10.1016/j.cellsig.2018.12.006
Received 18 October 2018; Received in revised form 10 December 2018; Accepted 11 December 2018
Available online 12 December 2018
0898-6568/

−511) sequence motif within the tumor necrosis factor α (*TNFA*) promoter, thereby activating transcription of *TNFA* upon LPS stimulation [5]. Various immune cells in LITAF knockdown and LITAF-deficient mice (macLITAF$^{-/-}$) manifest resistance to LPS-induced expression of some cytokines, including TNF-α, interleukin (IL)-6, IL-1β, and soluble TNF-α receptor II, and chemokine CXCL16 [6–8]. Apart from its important role in LPS-induced inflammation, LITAF is involved in inflammatory responses in arthritis, psoriasis, diabetes, and even cancers [9–12]. The effects of LITAF in PE pathogenesis have never been investigated. LITAF is highly expressed in the healthy placenta as compared with other organs, thus implying its important role in the development and functions of placenta [13]. Nevertheless, LITAF expression levels are further increased in the placenta of patients with PE relative to the healthy placenta, as indicated by a database [14]. This observation suggests that LITAF may also participate in PE pathogenesis.

A large number of noncoding RNAs, such as microRNAs (miRNAs) and long noncoding RNAs (lncRNAs), have recently garnered much attention owing to their important function in the modulation of gene expression, thereby participating in multiple pathological and physiological processes. MiRNAs are small (18–24 nt) endogenous single-stranded RNAs. It has been extensively demonstrated that miRNAs post-transcriptionally disrupt protein synthesis by binding to the untranslated region (3′UTR) of mRNAs and consequently inducing their degradation or preventing translation [15]. > 600 miRNAs have been found in the human placenta, constituting ~60% of all miRNAs that have been validated in humans [16,17]. Anomalous expression of specific miRNAs has been detected in the placenta of patients with PE [16]. A comparative analysis of PE-affected placentas and of healthy placentas has revealed that 34 miRNAs are deregulated in preeclamptic pregnancies, where miR-10b-3p has shown the most significant downregulation in the placentas affected by severe PE: decreasing to 28% of the level in healthy placentas [18]. Bioinformatic analysis has revealed that LITAF is a potential target of miR-10b-3p; thus, miR-10b-3p downregulation is likely responsible for the increased expression of LITAF in PE-affected placentas. LncRNAs are another type of noncoding RNAs and are normally longer than 200 nt. LncRNAs participate in complex molecular mechanisms that involve genetic imprinting, chromatin remodeling, splicing regulation, mRNA decay, and translational regulation [19]. One definite function of lncRNAs is their endogenous competitive sponging of mRNA from miRNAs, thereby protecting mRNA from miRNA-induced degradation [20]. Therefore, the interaction between lncRNAs and miRNAs plays an important part in the regulation of the expression of miRNA-targeted mRNAs.

This study was aimed at investigating the involvement of LITAF in PE pathogenesis and the regulatory effects of miR-10b-3p and lncRNAs on the expression of LITAF by *in vitro* and *in vivo* assays. The *in vitro* assay was performed on trophoblastic cells (HTR-8/SVneo cells) that were cultured under normoxic or hypoxic conditions. A mouse model of PE was established by the injection of the soluble form of the FLT-1 protein (sFLT-1). Our results are expected to facilitate further elucidation of the PE pathogenesis.

2. Materials and methods

2.1. Sample collection

Placentas were collected through cesarean delivery in a maternity unit in the Third Xiangya Hospital of the Central South University (Changsha, China) from March to October 2017. Ten samples from patients with PE and 10 samples from healthy controls were immediately frozen in liquid nitrogen after the surgical procedure and then were preserved at −80 °C. All protocols used in this study were approved by the Research Medical Ethics Committee of the Third Xiangya Hospital of Central South University. All women were informed of the research nature of our study and signed the informed consent forms. The characteristics of all patients and healthy controls are listed in Table 1.

Table 1
Clinical information on patients with PE and healthy controls.

Patient number	Age(years)	Gestational weeks	Urine protein (mg/24 h)	MAP (mmHg)
N1	26	38	_	95.25
N2	28	39 + 3	_	85.43
N3	31	39 + 2	_	89.36
N4	29	40 + 3	_	92.1
N5	34	39	_	96.17
N6	22	37 + 1	_	85.83
N7	30	35 + 6	_	89.31
N8	32	37	_	86.62
N9	27	38 + 4	_	97.86
N10	25	37 + 5	_	92.87
P1	33	31 + 4	4090	136.37
P2	25	33 + 3	1135	122.63
P3	34	31	3931	113.05
P4	27	34 + 3	1240	127.17
P5	24	28 + 4	2037	119.33
P6	28	34 + 3	162	121.67
P7	33	36 + 2	1536	131.4
P8	23	33 + 4	2493	115.33
P9	31	30 + 5	2499	118.2
P10	28	35 + 2	2803	117.33
P11	24	34 + 1	2018	120.67
P12	25	35 + 4	1764	112.67

N: normal controls; P: preeclampsia patients.

2.2. A reverse-transcription quantitative PCR (RT-qPCR) assay

Total RNA, including small RNA, was isolated from tissue samples or cells using the mirVana miRNA Kit (Thermo Fisher Scientific, Waltham, MA, USA). The cDNA was synthesized by means of the High Capacity RNA-to-cDNA Master Mix (Life Technologies, Carlsbad, CA, USA). The primers used in the qPCR experiments are shown in Table 2. The reaction was carried out on an ABI 7300 Real-Time PCR System (Applied Biosystems, Foster City, CA, USA) with the SYBR ExScript RT-PCR Kit (TaKaRa, Dalian, China). The qPCR thermal cycling conditions were as follows: a denaturation step of 30 s at 95 °C, followed by 40 cycles at 95 °C (5 s) and 60 °C (30 s). The expression levels of miRNAs and genes were normalized to those of *U6* and *GAPDH*, respectively, by the comparative threshold cycle ($2^{-\Delta\Delta CT}$) method.

2.3. A western blot assay

Total-protein samples from the placenta tissues and HTR-8/SVneo cells were extracted by homogenizing and lysing the samples in RIPA lysis buffer (Beyotime, Shanghai, China) supplemented with phenylmethanesulfonyl fluoride (PMSF, Beyotime), and then were denatured at 100 °C for 10 min. Total protein concentrations were determined with the BCA Reagent Kit (Beyotime). The protein samples (20 μg) were separated by sodium dodecyl sulfate polyacrylamide gel electrophoresis (SDS-PAGE) in a 10% or 12% gel and transferred to a polyvinylidene fluoride (PVDF) blotting membrane (Bio-Rad, Hercules, CA, USA). The membranes were blocked with nonfat dry milk (Yili Milk company, Inner Mongolia, China) at room temperature for 2 h and then hybridized with an anti-LITAF antibody (1:1000 dilution; cat. # ab187533, Abcam, Cambridge, UK), anti-FLT1 (Fms-like tyrosine kinase 1) antibody (1:500 dilution; ab184784, Abcam), and an anti-GAPDH antibody (dilution 1:2000, SC-365062, Santa Cruz Biotechnology, Dallas, TX, USA) at 4 °C overnight. Secondary biotin-conjugated antibodies were added to visualize the primary antibodies followed by detection *via* an avidin–biotin–peroxidase complex (Vectastain ABC Elite kit; Vector Laboratories Inc., Burlingame, CA, USA) and a substrate (Vector NovaRED, Vectastain). Densitometric

Table 2
The primer sequences for PCR.

Gene name	Sense (5'-3')	Antisense(5'-3')
has-lnc-MOCS2-1	CTGAATGGGATGCCTGAGAT	GGCAGGAGAAGAGGAAAACC
has-LNC-ASTE1	AGCCACCCTAACATGAGTGG	CATGAGAATGGCAAAGAGCA
has-WDR86-AS1	TCCTCTTAGGAACCGGTGAA	AGGTAAGGTCAGCGGTGTGT
has-EIF1B-AS1	CCCAAGGAAACAGGAGACAA	GCAACGGGCTTTCACATATT
has-lnc-TMEM160-1	GCATATGGCTTCTTCCTGCT	AGGAGGGGAGGTCAGGTTTA
has-LITAF	ATGTCGGTTCCAGGACCTTA	AAGGAGGATTCATGCCCTTC
has-FLT1	TGTCAATGTGAAACCCCAGA	GTCACACCTTGCTTCGGAAT
has-GAPDH	GGAGCGAGATCCCTCCAAAAT	GGCTGTTGTCATACTTCTCATGG
hsa-miR-10b-3p	ACACTCCAGCTGGGACAGATTCGATTCTAG	CTCAACTGGTGTCGTGGAGTCGGCAATTCAGTTGAGATTCCCCT
mmu-miR-10b-3p	ACACTCCAGCTGGGCAGATTCGATTCTAGG	CTCAACTGGTGTCGTGGAGTCGGCAATTCAGTTGAGTATTCCCC
U6	CTCGCTTCGGCAGCACA	AACGCTTCACGAATTTGCGT

analysis in the Quantity One software (Bio-Rad) was used to quantify the band intensities representing protein expression levels.

2.4. Cell culture and treatments

HTR-8/SVneo cells, purchased from ATCC (American Type Culture Collection, Manassas, VA), were cultured in the RPMI 1640 medium (Life Technologies, USA) supplemented with 10% of fetal bovine serum (Invitrogen, Carlsbad, CA, USA) and antibiotics (100 U/mL penicillin and 100 μg/mL streptomycin). Under normal conditions, cells were cultured in 75 cm^2 plastic flasks at 37 °C in a mixture of 5% CO_2, 20% O_2, and 75% N_2 as an atmosphere, whereas in the hypoxic condition, cells were cultured in an AW200SG hypoxic workstation (Electrotek, UK) with a continuous flow of a humidified mixture of 2% O_2, 5% CO_2, and 93% N_2 at 37 °*C. media* were refreshed every 2–3 days under both conditions.

2.5. Cell transfection

HTR-8/SVneo cells (10^5 cells/well) were seeded in 6-well plates. Small hairpin RNAs (shRNAs) targeting lncRNA WDR86-AS1 (shRNA-WDR86-AS1) and LITAF (shRNA-LITAF), the inhibitor and mimic oligonucleotides for *Homo sapiens* (has)-miR-10b-3p, and their negative controls were constructed by the GenePharma company (Shanghai, China). shRNA-WDR86-AS1, miR-10b-3p mimics, miR-10b-3p inhibitors, shRNA-LITAF, or relevant controls were transfected into HTR-8/SVneo cells using Lipofectamine 2000 (Invitrogen–Life Technologies). Briefly, Lipofectamine 2000 (5 μL) was diluted with 250 μL of serum-free Opti-MEM (31985–070, Gibco, Grand Island, NY, USA), followed by incubation at room temperature for 5 min. Next, 12.5 pmol of Bio-miRNA-NC, shRNA-WDR86-AS1, miR-10b-3p mimics, miR-10b-3p inhibitors, and shRNA-LITAF were diluted with 250 μL of serum-free Opti-MEM as well, and incubated at room temperature for 5 min. The two solutions were gently mixed, and the mixture was added into the wells. Following incubation at 37 °C for ~6–8 h, the cells were examined under a fluorescence microscope (XSP-BM13C, Shanghai Optical Instrument Factory, Shanghai, China).

2.6. A luciferase reporter assay

To identify a putative binding site (seed sequence) for hsa-miR-10b-3p in WDR86-AS1 and in the 3′UTR of *LITAF* mRNA, bioinformatics analysis was performed using TargetScan, miRanda, and PicTar. The wild-type (WT) WDR86-AS1 and LITAF 3′UTR as well as their mutant versions (MT), in which the putative binding sites were mutated, were synthesized and inserted into a pmirGLO vector (at *Xho*I and *Not*I restriction sites; Promega, Madison, WI, USA). The newly synthesized pmirGLO vectors were verified by DNA sequencing. HTR-8/SVneo cells (10^4 cells/well) were seeded in 12-well plates and transfected with the WT or MT constructs together with either hsa-miR-10b-3p mimics or negative control using Lipofectamine 2000 (Invitrogen). Cells were harvested at 48 h and the activity of firefly luciferase was measured and normalized to that of *Renilla* luciferase.

2.7. An RNA pull-down assay

Biotinylated RNA probes (Bio-miR-NC, Bio-miR-10b-3p and Bio-miR-10b-3p-Mut) were incubated with the lysates of HTR-8/SVneo cells and extracted by means of streptavidin-coupled magnetic beads according to the instructions for the Pierce™ Magnetic RNA Pull-Down Kit (Rockford, IL, USA). RNA–RNA complexes were then eluted with the salt solution and purified using TRIzol (Pierce). The enrichment of WDR86-AS1 in the RNA–RNA complexes was quantified by qPCR, as described above.

2.8. Microarray analyses

These analyses were performed on Human OneArray® v7 Microarrays (OneArray, Shanghai, China). Total mRNA was extracted with the RNeasy Kit (Qiagen) to prepare the cyanine 3 (Cy3)-labeled complementary RNA (cRNA). A total of 0.60 μg of Cy3-labeled cRNA was fragmented and hybridized to the Human Microarray for 17 h. Slides were washed and scanned immediately on an Agilent DNA Microarray Scanner (G2565CA) using the one-color scan setting for 8 × 60 K array slides. Scanned images were analyzed in Feature Extraction Software 10.10 (Agilent) with default parameters to obtain background-subtracted and spatially detrended processed signal intensities.

2.9. CCK-8 cell proliferation assay

Cell Counting Kit 8 (CCK-8, Dojindo Laboratories, Japan) was employed to measure cell viability. HTR-8/SVneo cells (0.5×10^4) were seeded in 96-well plates for 24 h. After the cell transfection, the cells were incubated under normoxia or hypoxia for 24 h. At 1 h before the end of incubation, 10 μL of the CCK-8 reagent was added into each well. Optical density (OD) at 490 nm in each well was determined on an enzyme immunoassay analyzer.

2.10. A Transwell cell invasion assay

This assay was conducted to examine the invasion ability of cells. HTR-8/SVneo cells (2×10^5) were seeded in the upper Transwell chamber (8 μm pore size; Corning, NY, USA). After cell transfection, the cells were incubated under normoxia or hypoxia for 48 h. Noninvading cells that remained on the top surface of the upper membrane were removed with a cotton-tipped swab. Invading cells on the reverse surface of the membrane were blocked with ice-cold methanol for 30 min and stained with 0.1% crystal violet. The stained cells were visualized by confocal microscopy and counted in 10 random visual fields per chamber (200× magnification).

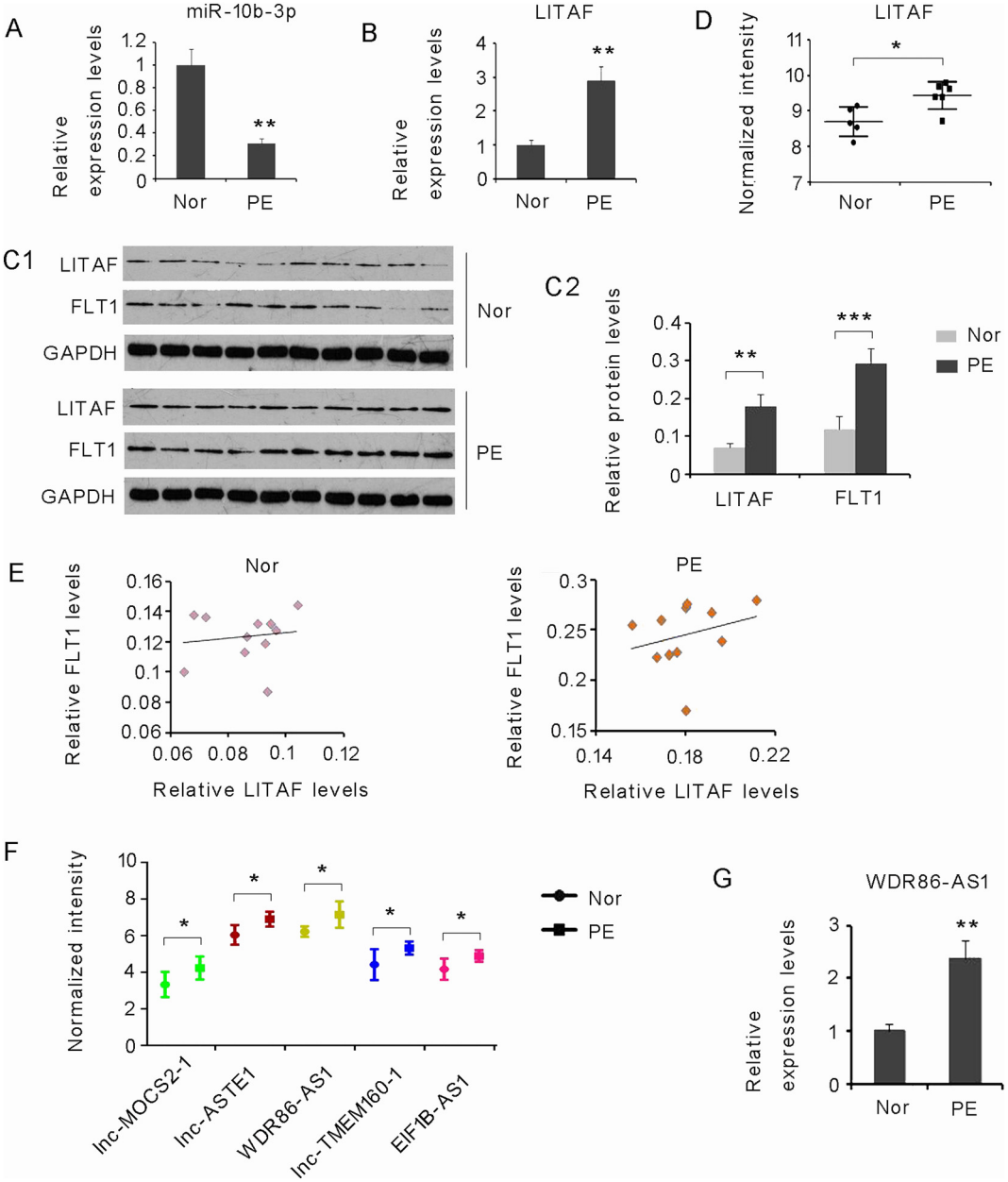

Fig. 1. Expression profiles of hsa-miR-10b-3p, LITAF, and WDR86-AS1 in the placentas of patients with PE and of healthy controls.
RT-PCR was performed to determine hsa-miR-10b-3p (A) and LITAF (B) expression in the placentas of patients with PE and of healthy controls. Western blot was performed to detect protein levels of LITAF and FLT1 in the placentas of patients with PE and of healthy controls (C). LITAF expression in GSE50783 datasets was analyzed (D). Association between LITAF and FLT1 expression levels was analyzed by the Pearson correlation analysis in healthy controls and patients with PE (E). Expression levels of five lncRNAs in GSE50783 datasets were analyzed (F). WDR86-AS1 expression was evaluated in the placentas of patients with PE and of healthy controls by RT-PCR. Nor: Normal group; PE: Preeclampsia group; *$p < .05$, **$p < .01$, ***$p < .001$ as compared with the control.

2.11. A scratch assay

HTR-8/SVneo cells were seeded in 6-well plates and cultured up to > 80% confluence. After the cell transfection, a scratch line was drawn on the cell monolayer by means of a 1 mL pipette tip. The cells were incubated in the FBS-free medium under normoxia or hypoxia for 48 h. Microscopic images of the same area were captured both during the hypoxic treatment and in the normoxic control. Cell migration was calculated based on the distance between initial and final positions.

2.12. Creation of the PE model

The animal experiment was approved by the Ethical Committee for Animal Research of the Central South University and adhered to the National Institutes of Health Guidelines for the care and use of animals. Pregnant C57/BL6N mice were obtained from Hunan SJA Co. (Changsha, China). The animals were housed in a temperature-controlled room (23 °C) on a 12 h:12 h light:dark cycle. Protein sFLT-1 (recombinant mouse VEGF R1/Flt-1 Fc Chimera, Cat. # 7756-FL-050, R &D Systems) was used to set up the mouse model of PE. From day 7 of gestation, sFLT-1 at 3.7 μg/kg per day (in sterile saline) was injected into a mouse tail vein for 6 days. The PE mice were injected with *Mus musculus* (mmu)-miR-10b-3p agomir ($n = 8$) or mmu-miR-agomir (n = 8) from the tail veins on day 13 of gestation at a rate of 100 μL/day for 6 days. Eight normal pregnant mice treated only with saline served as controls.

2.13. Blood pressure (BP) measurement and collection of tissues

Tail-cuff BP was measured noninvasively in conscious mice using a noninvasive automated sphygmomanometer (BP-98A, Softron, Beijing, China). Mice were incubated at 38 °C for 15 min to stabilize their physical parameters and to expand their local vessels sufficiently. The pressurized sensor was placed in their tails. Murine BP was measured after a few seconds of sobriety and tranquility. The average of five continuous measurements was registered as the final result for each mouse. To ensure relatively stable results, all BP measurements were performed at the same time of day every day during the experimental period. The protein concentrations in urine were measured on day 19 of gestation. Mice were euthanized under the anesthesia by an overdose of chloral hydrate. The urine was collected for subsequent analysis of protein concentrations by the Bradford method using a protein quantification kit (Beyotime). Placentas were collected for RT-qPCR and western blot assays as described above and/or for the immunohistochemical analysis described below.

2.14. Immunohistochemical staining

The placenta tissues were embedded in paraffin and sectioned into 4 μm slices, which were mounted on slides. Then, the slides were deparaffinized and hydrated. After inactivation of endogenous peroxidase in 3% hydrogen peroxide, antigens in slides were retrieved in citric acid buffer (pH 6.0) by microwaving for 15 min. Slides were blocked in normal goat serum (Invitrogen) for 30 min at room temperature, and then incubated with an anti-Ki67 antibody (Abcam) overnight at 4 °C. Samples were then washed with TBST (Invitrogen) and incubated with an appropriate secondary antibody (Abcam) for 2 h at 37 °C. After that, the sections were washed with TBST and stained by means of the DAB Detection Kit (Solarbio, Beijing, China). Finally, the sections were counterstained with hematoxylin. Images of sections were captured and analyzed using Motic Images Advanced 3.2 software (Motic, XiaMen, China).

2.15. A gelatin zymography assay

Gelatin zymography was performed to determine the activity of matrix metalloproteinases (MMP-2 and MMP-9) using the Gelatin Zymography Assay Kit (APPLYGEN, Beijing, China). The details have been described in another article [21]. The band intensity represented the activities of MMP-2 and MMP-9.

2.16. Statistical analysis

Data were analyzed in SPSS 12.0 software (SPSS, Inc., Chicago, IL, USA). One-way analysis of variance followed by Scheffe's *post hoc* test were performed to evaluate statistical significance ($p < .05$).

3. Results

3.1. Expression profiles of hsa-miR-10b-3p, LITAF, and WDR86-AS1 in PE-affected and healthy placentas

Our RT-qPCR analysis revealed that hsa-miR-10b-3p was downregulated in the PE-affected placentas, as compared to healthy placentas ($p < .01$, Fig. 1A); this result is in line with another report [18]. By contrast, LITAF was found to be upregulated in the placenta tissues from patients with PE ($p < .01$), as demonstrated by both RT-qPCR (Fig. 1B) and western blot assays (Fig. 1C). These data were in accord with those in the database record of GSE50783 (Fig. 1D). The FLT1 protein, an antiangiogenic factor, is biologically active and capable of causing endothelial dysfunction and the end organ dysfunction seen in PE. The FLT1 protein and its soluble form (sFLT-1) are upregulated respectively in the placenta and maternal circulation in PE; therefore, they are used for the clinical prediction and diagnosis of PE [22]. In this study, the FLT1 protein level was notably higher in the placentas of patients with PE than in the healthy placentas ($p < .001$, Fig. 1C). We found that there was significant correlation between LITAF and FLT1 in their protein levels in the PE-affected placentas ($p < .05$, $r = 0.469$, Fig. 1E). This correlation was not observed in the healthy placentas (Fig. 1E). To find an lncRNA that might influence the ability of miR-10b-3p to target mRNA, we searched all the lncRNAs that had putative binding sites for miR-10b-3p and were upregulated in the PE-affected placentas in dataset GSE50783. Five lncRNAs, including lnc-MOCS2–1, lnc-ASTE1, WDR86-AS1, lnc-TMEM160–1, and EIF1B-AS1, were found to meet the two requirements (Fig. 1F). Among them, WDR86-AS1 expression showed the most significant increase in the PE-affected placentas relative to healthy placentas. This study also identified aberrant upregulation of WDR86-AS1 in the PE-affected placentas ($p < .01$, Fig. 1G); thus, it was chosen for further experiments.

3.2. A regulatory network among hsa-miR-10b-3p, WDR86-AS1, and LITAF in trophoblast cells

A series of experiments was performed on the cultured trophoblast cells to determine whether there is a regulatory network among hsa-miR-10b-3p, WDR86-AS1, and LITAF. HTR-8/SVneo cells were transfected with shRNA-WDR86-AS1, miR-10b-3p inhibitors, miR-10b-3p mimics, or shRNA-LITAF to artificially change the expression of respective RNAs. Their transfection rates were evaluated through the comparisons of white-light images and fluorescent images; RNA expression was determined by RT-qPCR. The transfection with shRNA-WDR86-AS1, miR-10b-3p inhibitors, or shRNA-LITAF caused downregulation of WDR86-AS1 ($p < .01$, Fig. 2A), miR-10b-3p ($p < .01$, Fig. 2B), and LITAF ($p < .01$, Fig. 2D), respectively. However, miR-10b-3p was dramatically upregulated in the HTR-8/SVneo cells after the transfection with miR-10b-3p mimics ($p < .001$, Fig. 2C).

A knockdown of WDR86-AS1 caused miR-10b-3p upregulation ($p < .05$, Fig. 3A). Conversely, the upregulation of miR-10b-3p reduced WDR86-AS1 expression ($p < .05$, Fig. 3B). These data are suggestive of an inverse relation between WDR86-AS1 and miR-10b-3p. All the bioinformatic tools including TargetScan, miRanda, and PicTar identified a putative complementary region in WDR86-AS1 matching a region in miR-10b-3p. In the luciferase reporter assay, both the wild-type and mutant WDR86-AS1 constructs yielded increased luciferase activity as compared to the control ($p < .001$, Fig. 3C). By contrast, transfection with miR-10b-3p mimics significantly reduced the luciferase activity of the wild-type WDR86-AS1 constructs ($p < .01$), but not mutant WDR86-AS1 constructs; this finding confirmed the prediction of bioinformatic tools. In addition, the interaction between miR-10b-3p and WDR86-AS1 was identified by the RNA pull-down assay: significantly high relative WDR86-AS1 enrichment was observed only in the wild-type miR-10b-3p group, but not in the mutant group (Fig. 3D).

LITAF mRNA was predicted as a direct target of miR-10b-3p by the bioinformatic tools. Indeed, RT-qPCR analysis revealed a negative correlation between LITAF and miR-10b-3p: LITAF expression significantly increased with a reduction in miR-10b-3p levels ($p < .01$, Fig. 4A), but LITAF expression decreased when miR-10b-3p was upregulated ($p < .01$, Fig. 4A). Moreover, the transfection with miR-10b-3p mimics significantly reduced luciferase activity of the wild-type *LITAF* 3′UTR constructs ($p < .01$, Fig. 4B) but not that of the mutant construct.

3.3. Hypoxia changed WDR86-AS1, hsa-miR-10b-3p, and LITAF expression in the trophoblast cells

To mimic the growth of trophoblast cells in the hypoxic state in patients with PE, HTR-8/SVneo cells were cultured in the low-oxygen condition. The relative RNA expression levels of WDR86-AS1 and *LITAF*

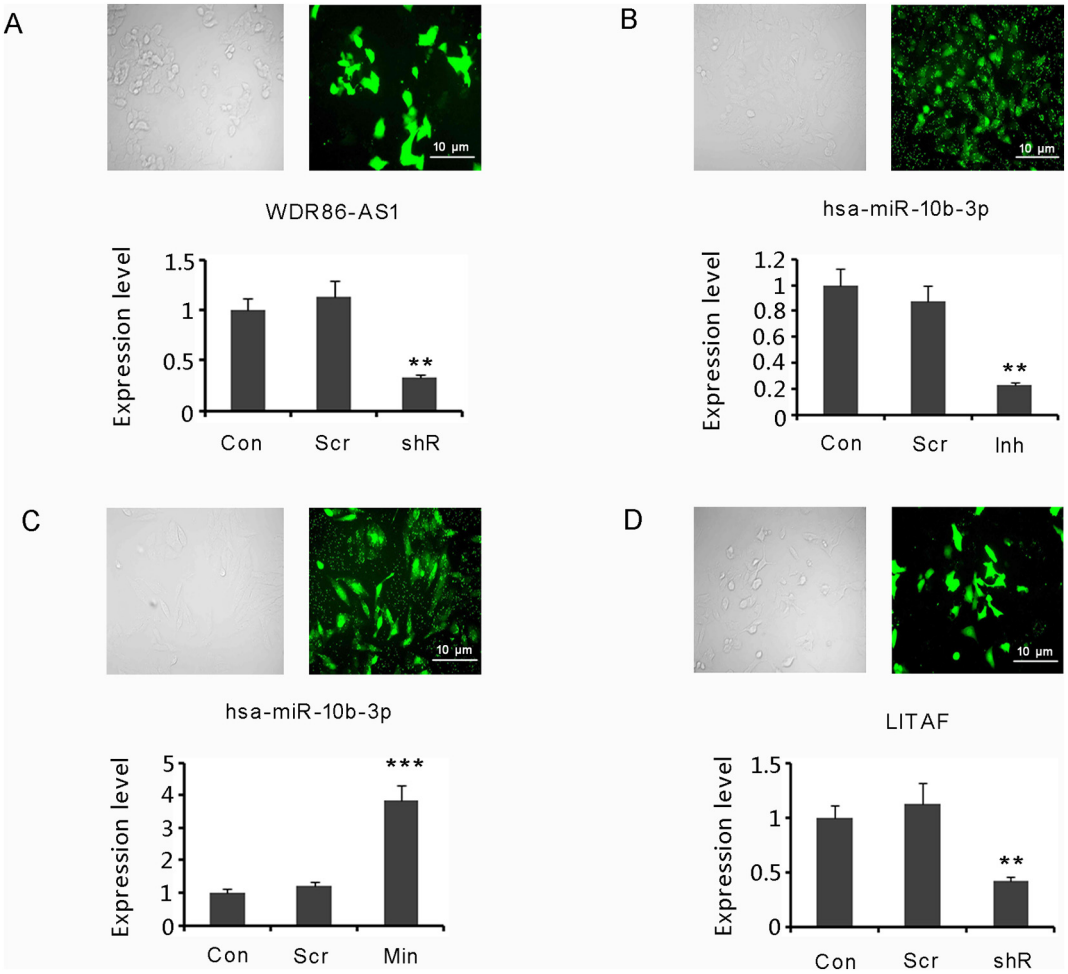

Fig. 2. Alterations of WDR86-AS1, hsa-miR-10b-3p, and LITAF expression in trophoblast cells after the transfection procedures.
HTR-8/SVneo cells were transfected with shRNA-WDR86-AS1 (A), hsa-miR-10b-3p inhibitors (B), hsa-miR-10b-3p mimics (C), shRNA-LITAF (D), or their negative controls. The transfection rate was determined by the white-light and fluorescent images. WDR86-AS1, hsa-miR-10b-3p, and LITAF expression levels were assessed by PT-PCR. Con: control; Scr: the scrambled control shRNA; shR: the shRNA; Inh: inhibitors; Mim: Mimics. *$p < .05$, **$p < .01$, ***$p < .001$ as compared with the control.

were significantly higher in the HTR-8/SVneo cells in the hypoxic condition than in the normoxic condition ($p < .01$, Fig. 5A). By contrast, the hsa-miR-10b-3p expression level was lower under hypoxia ($p < .01$, Fig. 5A). We next investigated the effect of the WDR86-AS1/hsa-miR-10b-3p/LITAF network on LITAF protein levels in the HTR-8/SVneo cells in the hypoxic condition. LITAF protein level increased under hypoxia ($p < .05$, Fig. 5B); this finding was consistent with the change at mRNA levels. Nonetheless, transfection with shRNA-WDR86-AS1 ($p < .01$ *vs.* hypoxic group), hsa-miR-10b-3p mimics ($p < .01$ *vs.* hypoxic group), or shRNA-LITAF ($p < .001$ *vs.* hypoxic group) attenuated the LITAF upregulation observed under hypoxia. The hsa-miR-10b-3p inhibitors further increased LITAF protein levels under hypoxia ($p < .01$ *vs.* hypoxic group).

To identify the genes that are regulated by LITAF under hypoxia, we knocked down the *LITAF* gene and then detected the changes in the gene expression in the microarray experiment. The Human OneArray® v7 Microarray contains 29,204 probes. The results revealed that the expression levels of 769 genes underwent fold changes of > 2.0-fold in HTR-8/SVneo cells under hypoxia after the depletion of LITAF. Among these genes, 574 were downregulated and 195 were upregulated in the LITAF-depleted cells (Fig. 5C). The top-ten most strongly up-regulated genes were *PLAU*, *COL17A1*, *PLAT*, *VCAN*, *GPC6*, *MMP14*, *STAT1*, *TGFBR1*, *TNC*, and *C1orf112* (Table 3). The top-ten most strongly down-regulated genes were *TNF-a*, *TNF-R2*, *TLR4*, *CXCL16*, *CCR8*, *COL6*, *TNFAIP3*, *TNF-R1*, *CCL19*, and *IL6* (Table 4). The list of top-ranking biological processes affected by LITAF depletion is presented in Table 5.

3.4. The WDR86-AS1/hsa-miR-10b-3p/LITAF network modulates the viability, migration, and invasiveness of HTR-8/SVneo cells under hypoxia

HTR-8/SVneo cell viability was inhibited by hypoxia ($P < .05$, Fig. 6A), but the WDR86-AS1 or LITAF knockdown or hsa-miR-10b-3p overexpression partly restored the cell viability (all $p < .05$ *vs.* hypoxic group). Similarly, hypoxia attenuated the migration and invasiveness of HTR-8/SVneo cells ($p < .01$ and $p < .001$ respectively, Fig. 6B and C). On the other hand, the inhibition of migration and invasion was partly reversed by the WDR86-AS1 or LITAF knockdown or by hsa-miR-10b-3p overexpression.

3.5. Increased miR-10b-3p expression attenuates PE symptoms in the mouse model

The mouse model of PE was set up using sFLT-1 injection. The mean arterial pressure (MAP) gradually increased from day 13 of gestation and reached its peak of ~150 on day 18 in the PE-affected pregnant mice ($p < .001$, Fig. 7C). The urinary protein concentration in the PE-affected pregnant mice dramatically increased ($p < .001$, Fig. 7D), and these mice showed a reduction in the fetal survival rate ($p < .01$,

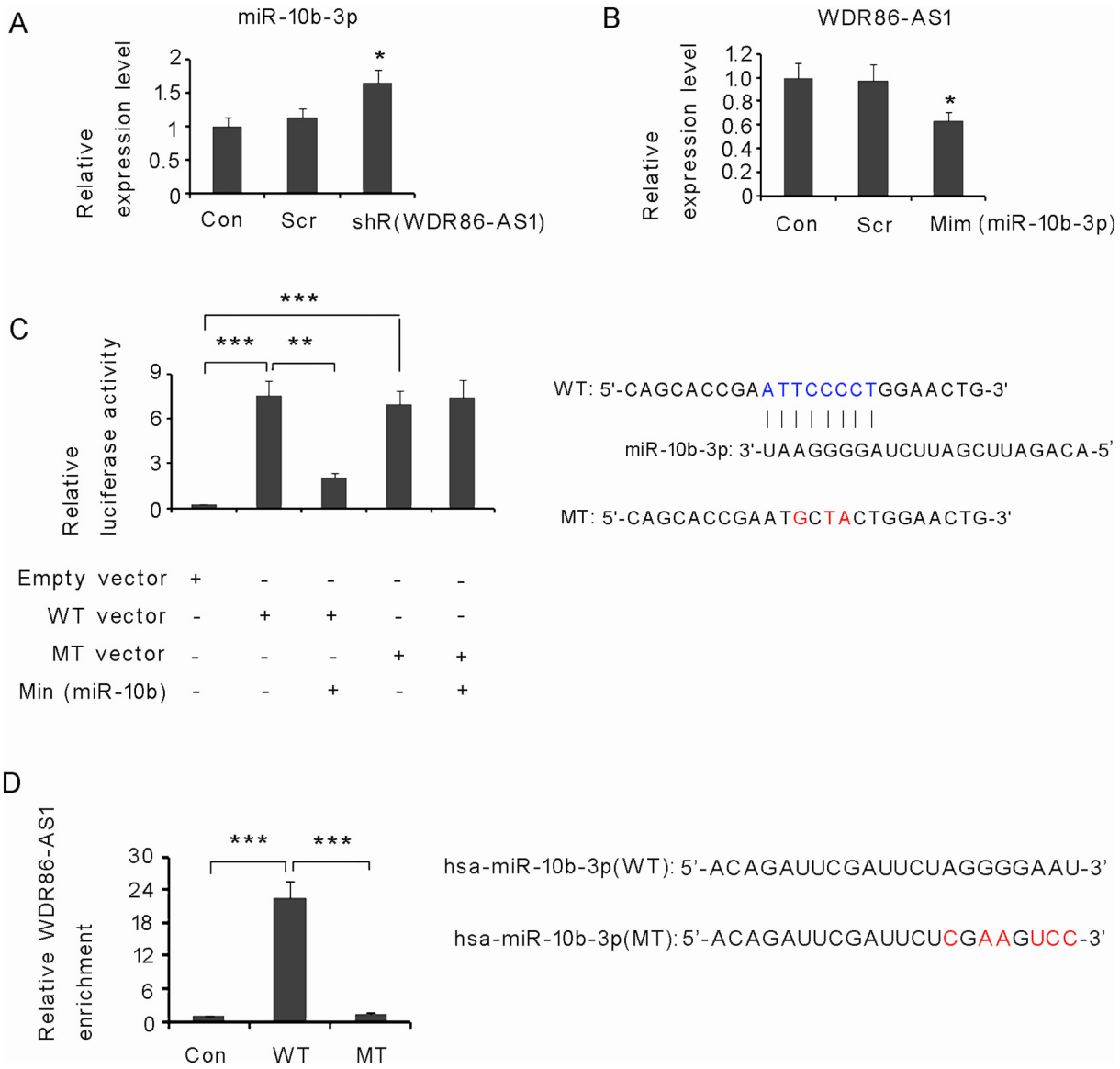

Fig. 3. Negative correlation between WDR86-AS1 and hsa-miR-10b-3p expression levels in trophoblast cells.
Hsa-miR-10b-3p expression in the trophoblast cells was analyzed by RT-PCR after a WDR86-AS1 knockdown (A); WDR86-AS1 expression in the trophoblast cells was analyzed by RT-PCR after transfection with hsa-miR-10b-3p mimics (B). In a luciferase reporter assay, transfection with hsa-miR-10b-3p mimics significantly reduced the luciferase activity of the wild-type WDR86-AS1 constructs, but not that of the mutant WDR86-AS1 constructs (C). RNA pull-down analysis indicated that WDR86-AS1 interacted with WT-hsa-miR-10b-3p, but not with MT-hsa-miR-10b-3p (D). $*p < .05$, $**p < .01$ and $***p < .001$ as compared with the control.

Fig. 7E). All these data indicated that the mouse model of PE was created successfully. MiR-10b-3p expression decreased in the placentas of mice with PE ($p < .01$, Fig. 7A), as indicated by RT-qPCR. To determine the effect of miR-10b-3p in the PE pathogenesis, the mice were injected with mmu-miR-10b-3p agomir, which abrogated the downregulation of miR-10b-3p in the mice with PE ($p < .01$ *vs.* sFLT-1 group). Western blot analysis uncovered a remarkable increase in LITAF expression in the placentas of the mouse model of PE ($p < .001$, Fig. 7B), however, the injection with mmu-miR-10b-3p agomir reversed the LITAF upregulation in the PE mice ($p < .001$ *vs.* sFLT-1 group). Attenuation of the miR-10b-3p downregulation in the mice with PE inhibited the increase in MAP expression ($p < .01$, *vs.* sFLT-1 group) and urinary protein concentration ($p < .05$ *vs.* sFLT-1 group) and attenuated the reduction in the fetal survival rate ($p < .05$, *vs.* sFLT-1 group). We tested Ki67 expression in the placentas by immunohistochemical staining because Ki67 expression is an important indicator of cell proliferation. Although Ki67 expression decreased in the placentas of mice with PE, the injection with mmu-miR-10b-3p agomir reversed the Ki67 downregulation in some cells (Fig. 7F). An MMP zymographic assay was performed to evaluate the activities of MMP-2 and MMP-9 in the placentas. Activities of MMP-2 ($p < .05$, Fig. 7G) and MMP-9 ($p < .01$) were lower in the mice with PE, but this decrease was partly reversed after the injection with mmu-miR-10b-3p agomir.

4. Discussion

Aberrant expression of lncRNAs and miRNAs has been detected in the placentas of patients with PE as compared to healthy controls [16,18]. Although these noncoding RNAs are not translated to proteins, they play an important role in the modulation of mRNA translation. Therefore, many lncRNAs and miRNAs have received increasing attention because of their potential participation in PE pathogenesis [23–25]. Hsa-miR-10b-3p has shown the most significant downregulation in PE-affected placentas in another comparative analysis [18]. The present study also uncovered downregulation of hsa-miR-

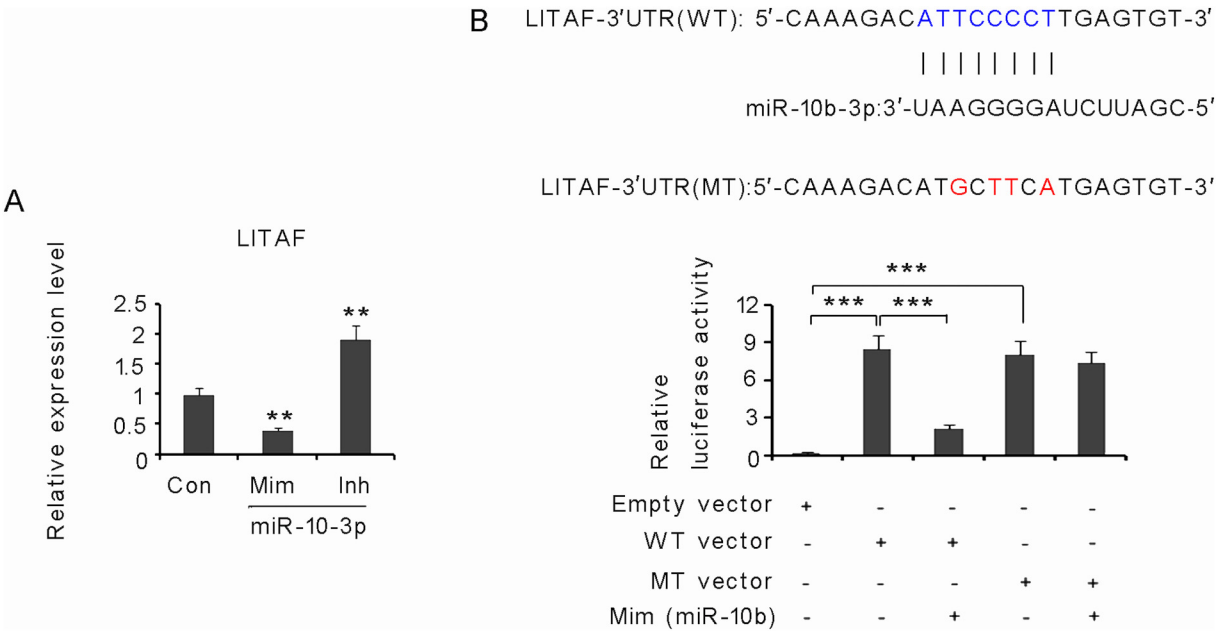

Fig. 4. *LITAF* mRNA is a direct target of miR-10b-3p.
LITAF expression in the trophoblast cells was assessed after the transfection with miR-10b-3p mimics (Mim) or inhibitors (Inh) (A). In a luciferase reporter assay, transfection with miR-10b-3p mimics significantly reduced the luciferase activity of the wild-type LITAF constructs, but not that of the mutant LITAF constructs (B). $^{**}p < .01$ and $^{***}p < .001$ as compared with the control.

10b-3p in PE. Conversely, *LITAF*, as a putative target of miR-10b-3p, was upregulated in the placentas of patients with PE. Thus, the miR-10b-3p downregulation might be responsible for the anomalous increase in *LITAF* expression in PE. LncRNAs can interfere with the targeting of mRNA by miRNA by competitively binding to miRNAs, a process termed “sponge adsorption” [20]. We found that five candidate lncRNAs that potentially bind to miR-10b-3p, were upregulated in the placentas of patients with PE in a database (dataset GSE50783, see reference [14]), among which WDR86-AS1 showed the greatest upregulation. Upregulated WDR86-AS1 likely increases LITAF expression in PE by sponging miR-10b-3p.

A series of experiments was next conducted in this study to identify the associations within the WDR86-AS1/miR-10b-3p/LITAF network. This study proves a specific binding between WDR86-AS1 and miR-10b-3p by luciferase reporter and RNA pull-down assays. Furthermore, we found a negative correlation between WDR86-AS1 and miR-10b-3p in terms of their expression in trophoblast cells, although the underlying mechanism is not fully understood. Mo et al. have found that lncRNA GAPLINC contains a binding site for miR-382-5p and miR-575; a GAPLINC knockdown upregulated miR-382-5p and miR-575 in fibroblast-like synoviocytes [26]. LncRNA SNHG16 contains a binding sequence complementary to the seed region of miR-4518. Overexpression of SNHG16 significantly represses the expression of miR-4518, whereas silencing of SNHG16 leads to the upregulation of miR-4518 in breast cancer U251 and LN229 cells [27]. Our luciferase reporter assay also revealed that miR-10b-3p binds to the 3′UTR of *LITAF* mRNA. It has been well established that miRNAs induce mRNA degradation after binding to the 3′UTR of mRNA in an RNA-induced silencing complex (RISC) [28,29]. In line with the data from the luciferase reporter assay, an inverse relation was seen between miR-10b-3p and LITAF: significantly lower relative mRNA expression of LITAF was observed after miR-10b-3p mimic treatment but higher expression after the miR-10b-3p inhibitor treatment. This result suggests that LITAF is negatively regulated by miR-10b-3p but may positively correlate with WDR86-AS1 expression.

Early placental development occurs in an environment of relative hypoxia. Nonetheless, hypoxia, especially after the placental perfusion has been fully established, causes trophoblast injury and contributes to the pathophysiology of placental dysfunction and fetal growth restriction in PE [30]. Thus, an *in vitro* PE model is usually studied under hypoxic conditions [31]. In the present study, HTR-8/SVneo cells under hypoxia showed higher WDR86-AS1 and LITAF expression but lower miR-10b-3p levels relative to the cells under normoxia, suggesting that hypoxia is an important cause of their aberrant expression in the PE-affected placentas. Some reports suggest that hypoxia disturbs expression of many miRNAs and mRNAs in human cytotrophoblasts [32–34]. Our WDR86-AS1 knockdown and miR-10b-3p overexpression abrogated the upregulation of LITAF in HTR-8/SVneo cells under hypoxia, suggesting that WDR86-AS1 and miR-10b-3p mediated the LITAF upregulation under hypoxia.

In this study, we blocked the upregulation of LITAF under hypoxia by RNA interference, to understand the biological or pathological roles of LITAF in the trophoblastic cells. Data from the microarray experiments revealed that expression levels of certain genes and some biological processes significantly changed after LITAF depletion. In the LITAF-depleted cells, the most downregulated genes, such as *TNFA*, *TNFR2*, *TLR4*, and *CXCL16*, are associated with inflammatory responses, suggesting that LITAF plays a critical proinflammatory part in trophoblastic cells under hypoxia. The most upregulated genes, such as *PLAU*, *PLAT*, and *MMP14*, after LITAF depletion are implicated in the degradation of the extracellular matrix. Other upregulated genes like STAT1 and TGFBR1 are involved in the control over cell proliferation, differentiation, and apoptosis. Besides, the significantly affected biological processes involved the Toll-like receptor signaling pathway, leukocyte transendothelial migration, extracellular matrix–receptor interaction, the chemokine signaling pathway, focal adhesion, apoptosis, tight junctions, regulation of the actin cytoskeleton, FcγR–mediated phagocytosis, and the cell cycle. These data shed light on the extensive participation of LITAF in the modulation of inflammatory responses, cell migration, and proliferation under hypoxia.

This study revealed that the WDR86-AS1/miR-10b-3p/LITAF network regulates the viability, migration, and invasiveness of HTR-8/SVneo cells under hypoxia. Chronic and severe hypoxia impairs the viability, migration, and invasiveness of trophoblast cells, although mild hypoxia is important for the modulation of the survival, differentiation, and metabolic function of trophoblast cells in early placental

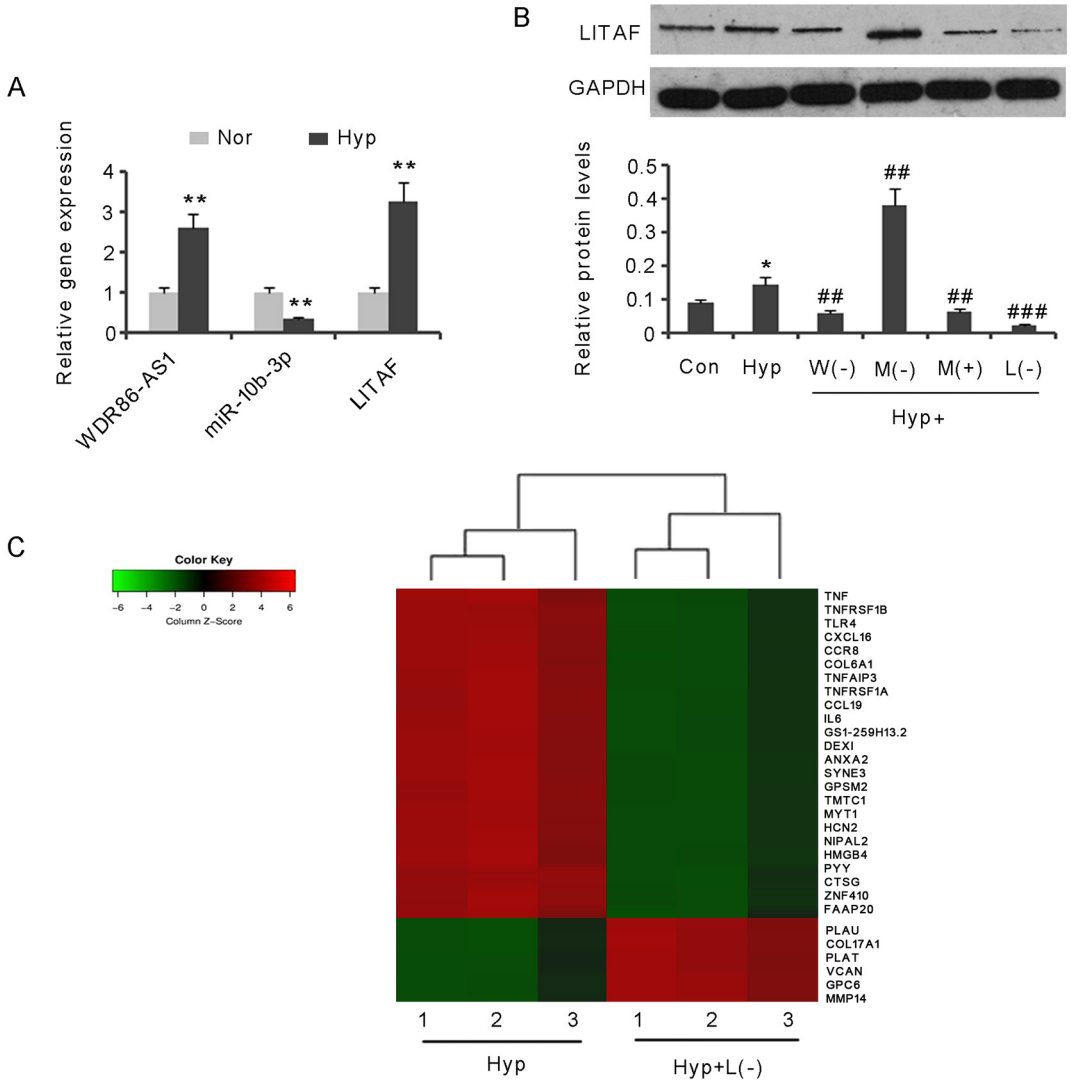

Fig. 5. Expression profiles of WDR86-AS1, hsa-miR-10b-3p, LITAF, and LITAF-regulated genes in the trophoblast cells under hypoxia.
Expression profiles of WDR86-AS1, hsa-miR-10b-3p, and LITAF were determined by RT-PCR in the trophoblast cells under hypoxia or normoxia (A). Western blotting was performed to evaluate LITAF expression in the trophoblast cells under the hypoxia after transfection with shRNA-WDR86-AS1, hsa-miR-10b-3p inhibitors, hsa-miR-10b-3p mimics, or shRNA-LITAF (B). A microarray experiment was performed on the trophoblast cells under hypoxia after LITAF was knocked down or not (C). Hyp: hypoxia; Nor: normoxia. $^{*}p < .05$, $^{**}p < .01$ as compared with the HTR-8/SVneo cells under normoxia; $^{\#}p < .05$, $^{\#\#}p < .01$ as compared with the HTR-8/SVneo cells under hypoxia.

development. Decreased viability, migration, and invasiveness of trophoblast cells are associated with inadequate vascular remodeling, which is a leading cause of consequent pathological changes such as reduced uteroplacental perfusion, oxidative stress, and excessive inflammation [3,4]. The present study showed that normalizing the expression of WDR86-AS1, miR-10b-3p, and LITAF under hypoxia to some extent restored the cell viability, migration, and invasion of trophoblast cells. This finding suggests that the disturbance of their expression adversely affects these properties of trophoblast cells. Some cancer studies have revealed the regulatory effects of miR-10b-3p and

Table 3
The most strongly upregulated genes in the LITAF-depleted cells under hypoxia.

Gene symbol	Description	Log_2 (Ratio)	*P* value (for differential expression)
PLAU	*Homo sapiens* plasminogen activator, urokinase	5.64385619	3.53E-05
COL17A1	*Homo sapiens* collagen, type XVII, alpha 1	4.532905585	6.27E-05
PLAT	*Homo sapiens* plasminogen activator, tissue	4.399167018	7.03E-05
VCAN	*Homo sapiens* versican	4.343245623	7.59E-05
GPC6	*Homo sapiens* glypican 6	4.315432619	8.23E-05
MMP14	*Homo sapiens* matrix metallopeptidase 14 (membrane-inserted)	4.26986112	8.73E-05
STAT1	*Homo sapiens* signal transducer and activator of transcription 1	4.23585619	8.92E-05
TGFBR1	*Homo sapiens* transforming growth factor, beta receptor 1	4.21504582	9.14E-05
TNC	*Homo sapiens* tenascin C	4.19387745	9.57E-05
C1orf112	*Homo sapiens* chromosome 1 open reading frame 112	4.16479563	3.32E-0.4

Table 4
The most strongly downregulated genes in the LITAF-depleted cells under hypoxia.

Gene symbol	Description	Log_2 (Ratio)	P value (for differential expression)
TNF-a	*Homo sapiens* tumor necrosis factor, alpha	−6.64385619	1.53E-07
TNF-R2	*Homo sapiens* tumor necrosis factor receptor superfamily, member 2	−6.532905585	6.27E-07
TLR4	*Homo sapiens* toll-like receptor 4	−6.339167018	9.73E-07
CXCL16	*Homo sapiens* chemokine (C-X-C motif)	−6.17385619	1.93E-06
CCR8	*Homo sapiens* chemokine (C−C motif) receptor 8	−6.0456832	3.16E-06
COL6	*Homo sapiens* CC chemokine ligands 6	−5.9664976	3.73E-06
TNFAIP3	*Homo sapiens* tumor necrosis factor, alpha-induced protein 3	−5.94385619	4.22E-06
TNF-R1	*Homo sapiens* tumor necrosis factor receptor superfamily, member 1	−5.92521582	4.67E-06
CCL19	*Homo sapiens* CC chemokine ligands 19	−5.87438757	5.13E-06
IL6	*Homo sapiens* interleukin 6	−5.81749775	5.97E-06

Table 5
The top-ranking biological processes after LITAF depletion.

Geneset name	# genes in geneset (K)	# genes in overlap (k)	p value
hsa04620:Toll-like receptor signaling pathway	201	69	2.38E-05
hsa04670:Leukocyte transendothelial migration	67	29	1.27E-04
hsa04512:ECM-receptor interaction	84	34	1.40E-04
hsa04062:Chemokine signaling pathway	17	12	1.44E-04
hsa04510:Focal adhesion	28	17	3.56E-04
hsa04210:Apoptosis	24	14	4.36E-04
hsa04530:Tight junction	34	25	1.31E-03
hsa04810:Regulation of actin cytoskeleton	85	31	2.17E-03
hsa04666:Fc gamma R-mediated phagocytosis	55	24	3.52E-03
hsa04110:Cell cycle	40	17	5.90E-03

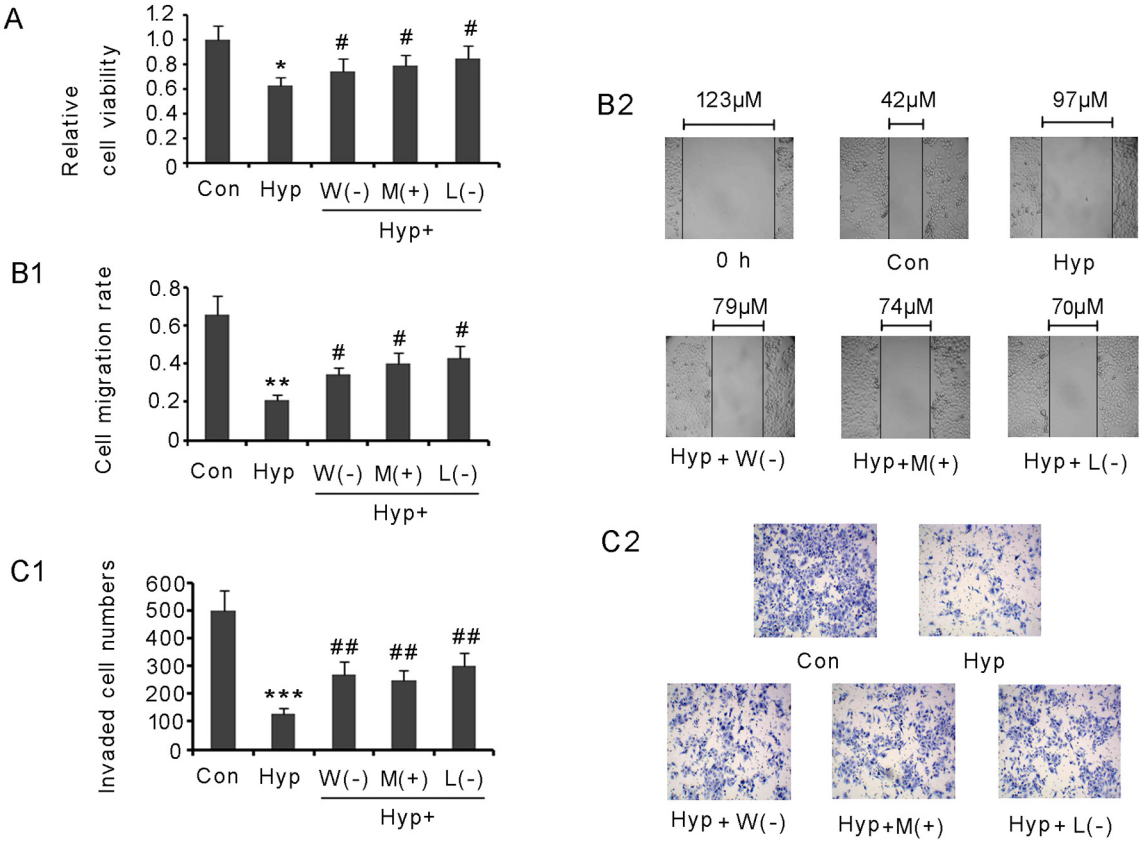

Fig. 6. WDR86-AS1, hsa-miR-10b-3p, and LITAF regulate the growth properties and invasiveness of trophoblast cells under hypoxia.
HTR-8/SVneo cells were transfected with shRNA-WDR86-AS1, hsa-miR-10b-3p mimics, or shRNA-LITAF under hypoxia. After 48 h, cell viability (A), the migration rate (B), and invasion rate (C) of the cells were evaluated. W(−): the WDR86-AS1 knockdown; M(+): miR-10b-3p overexpression; L(−): a LITAF knockdown; Hyp: hypoxia; Con: normoxia. $^{*}p < .05$, $^{**}p < .01$ as compared with the HTR-8/SVneo cells under normoxia; $^{\#}p < .05$, $^{\#\#}p < .01$ as compared with the HTR-8/SVneo cells under hypoxia.

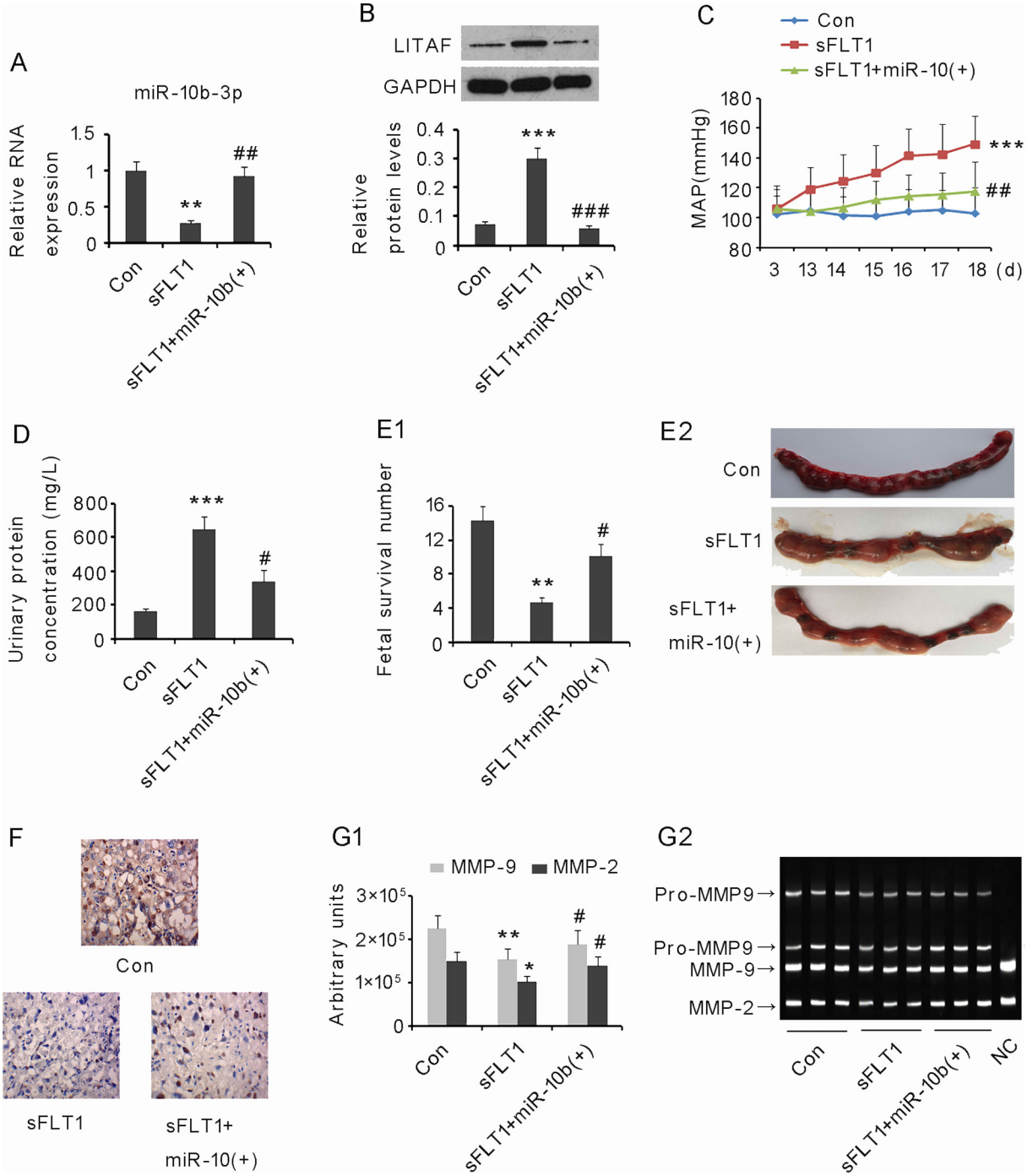

Fig. 7. Increased miR-10b-3p expression reversed PE symptoms in the mouse model.
The mouse model of PE was set up by means of sFLT-1. Some mice with PE were injected with mmu-miR-10b-3p agomir to increase mmu-miR-10b-3p expression. miR-10b-3p expression in placentas was assessed *via* RT-PCR (A). Protein levels of LITAF in placentas were assessed by western blotting (B). Blood pressure (C), urine protein concentrations (D), and fetal survival rate of the mice (E) were recorded. Ki67 expression in placentas was assessed by immunohistochemical staining. Gelatin zymography was performed to determine the activity of matrix metalloproteinases (MMP)-2 and − 9 (F). $^{*}p < .05$, $^{**}p < .01$ as compared with the control; $^{\#}p < .05$, $^{\#\#}p < .01$ as compared with the sFLT-1 group.

LITAF on cell proliferation and migration [35–38]. Upregulation of miR-10b-3p increases the proliferative, migratory, and invasive abilities of hepatocellular carcinoma cells [35]. LITAF not only is a modulator of an inflammatory response but also functions as a tumor suppressor in B-cell non-Hodgkin's lymphoma, pancreatic cancer, and prostate cancer [36–38]. The ectopic expression of LITAF induces tumor cell apoptosis, but a knockdown of LITAF robustly protects tumor cells from apoptosis [36–38]. These data are in line with the regulatory effects of miR-10b-3p and LITAF in trophoblast cells.

The mouse model of PE in this study was created by the injection of sFLT-1. The latter is a well-recognized mediator of the pathogenesis of PE. Circulating levels of sFLT-1 are elevated in the serum of women with PE. It is thought that the source of circulating sFLT-1 in patients with PE is primarily the placenta in response to a variety of stimuli, particularly hypoxia [39]. sFLT-1 works as an antiangiogenic factor by antagonizing the actions of proangiogenic factors such as vascular

endothelial growth factor and placental growth factor [40]. Exogenous administration of sFLT-1 to pregnant mice induces widespread endothelial dysfunction, oxidative stress, inflammation, and apoptosis in trophoblasts [41]. The present study suggests that sFLT-1 injection into pregnant mice causes notable elevation in maternal BP and urinary protein concentration but a reduction in the fetal survival rate, which are hallmarks of PE. MiR-10b-3p turned out to be downregulated in the placenta of sFLT-1–injected mice, with LITAF being upregulated. Co-treatment with mmu-miR-10b-3p agomir to restore miR-10b-3p expression attenuated the pathological changes caused by sFLT-1, thus pointing to a protective effect of miR-10b-3p against PE. We found that upregulation of miR-10b-3p in the mouse model of PE increased Ki67 expression and activities of MMP-2 and -9, indicating increased viability and migration of trophoblast cells. This phenomenon likely is an important mechanism underlying the protective effects of miR-10b-3p.

In summary, WDR86-AS1, miR-10b-3p, and LITAF are all involved in PE pathogenesis. Their aberrant expression may disturb the regulatory relations in the WDR86-AS1/miR-10b-3p/LITAF network, thereby probably triggering PE pathogenesis during pregnancy.

Acknowledgements

None.

Disclosure of interests

The authors declare that they have no conflicts of interest.

Contribution to authorship

Ruizhen Li conducted the experiments and wrote the manuscript. Min Xue took the responsibility of the line-editing and proofreading.

Details of ethics approval

All protocols used in this study were approved by the Research Medical Ethics Committee of the Third Xiangya Hospital of the Central South University. All women were informed of the research nature of our study with informed consent forms signed. The animal experiment was approved by the Ethical Committee for Animal Research of Central South University and adhered to National Institutes of Health Guidelines for the care and use of animals.

Funding

None.

References

[1] K. Duhig, B. Vandermolen, A. Shennan, Recent advances in the diagnosis and management of pre-eclampsia, F1000Res 7 (2018) 242.
[2] U.V. Ukah, D.A. De Silva, B. Payne, L.A. Magee, J.A. Hutcheon, H. Brown, J.M. Ansermino, T. Lee, P. von Dadelszen, Prediction of adverse maternal outcomes from pre-eclampsia and other hypertensive disorders of pregnancy: a systematic review, Pregnancy Hypertens. 11 (2018) 115–123.
[3] S.J. Fisher, Why is placentation abnormal in preeclampsia? Am. J. Obstet. Gynecol. 213 (4 Suppl) (2015) S115–S122.
[4] A.L. Winship, K. Koga, E. Menkhorst, M. Van Sinderen, K. Rainczuk, M. Nagai, C. Cuman, J. Yap, J.G. Zhang, D. Simmons, M.J. Young, E. Dimitriadis, Interleukin-11 alters placentation and causes preeclampsia features in mice, Proc. Natl. Acad. Sci. U. S. A. 112 (52) (2015) 15928–15933.
[5] J. Zou, P. Guo, N. Lv, D. Huang, Lipopolysaccharide-induced tumor necrosis factor-α factor enhances inflammation and is associated with cancer (Review), Mol. Med. Rep. 12 (5) (2015) 6399–6404.
[6] X. Tang, S. Amar, Kavain inhibition of LPS-induced TNF-α via ERK/LITAF, Toxicol Res (Camb). 5 (1) (2016) 188–196.
[7] S. Ceccarelli, N. Panera, M. Mina, D. Gnani, C. De Stefanis, A. Crudele, C. Rychlicki, S. Petrini, G. Bruscalupi, L. Agostinelli, L. Stronati, S. Cucchiara, G. Musso, C. Furlanello, G. Svegliati-Baroni, V. Nobili, A. Alisi, LPS-induced TNF-α factor mediates pro-inflammatory and pro-fibrogenic pattern in non-alcoholic fatty liver disease, Oncotarget 6 (39) (2015) 41434–41452.
[8] K.N. Bushell, S.E. Leeman, E. Gillespie, A.C. Gower, K.L. Reed, A.F. Stucchi, J.M. Becker, S. Amar, LITAF mediation of increased TNF-α secretion from inflamed colonic lamina propria macrophages, PLoS One 6 (9) (2011) e25849.
[9] W.J. Chang, X.P. Niu, R.X. Hou, J.Q. Li, R.F. Liu, Q. Wang, C.F. Wang, X.H1. Li, G.H. Yin, K.M. Zhang, LITAF, HHEX, and DUSP1 expression in mesenchymal stem cells from patients with psoriasis, Genet. Mol. Res. 14 (4) (2015) 15793–15801.
[10] Z.Z. Ji, Z. Dai, Y.C. Xu, A new tumor necrosis factor (TNF)-α regulator, lipopolysaccharides-induced TNF-α factor, is associated with obesity and insulin resistance, Chin. Med. J. 124 (2) (2011) 177–182.
[11] J.C. Merrill, J. You, C. Constable, S.E. Leeman, S. Amar, Whole-body deletion of LPS-induced TNF-α factor (LITAF) markedly improves experimental endotoxic shock and inflammatory arthritis, Proc. Natl. Acad. Sci. U. S. A. 108 (52) (2011) 21247–21252.
[12] C. Hoey, J. Ray, J. Jeon, X. Huang, S. Taeb, J. Ylanko, D.W. Andrews, P.C. Boutros, S.K. Liu, miRNA-106a and prostate cancer radioresistance: a novel role for LITAF in ATM regulation, Mol. Oncol. (2018).
[13] K.N. Bushell, S.E. Leeman, E. Gillespie, A.C. Gower, K.L. Reed, A.F. Stucchi, J.M. Becker, S. Amar, LITAF mediation of increased TNF-α secretion from inflamed colonic lamina propria macrophages, PLoS One 6 (9) (2011) e25849.
[14] X. He, Y. He, B. Xi, J. Zheng, X. Zeng, Q. Cai, Y. Ouyang, C. Wang, X. Zhou, H. Huang, W. Deng, S. Xin, Q. Huang, H. Liu, LncRNAs expression in preeclampsia placenta reveals the potential role of LncRNAs contributing to preeclampsia pathogenesis, PLoS One 8 (11) (2013) e81437.
[15] W. Sun, Y.S. Julie Li, H.D. Huang, J.Y. Shyy, S. Chien, microRNA: a master regulator of cellular processes for bioengineering systems, Annu. Rev. Biomed. Eng. 12 (2010) 1–27.
[16] C. Munaut, L. Tebache, S. Blacher, A. Noël, M. Nisolle, F. Chantraine, Dysregulated circulating miRNAs in preeclampsia, Biomed Rep. 5 (6) (2016) 686–692.
[17] M.R. Friedländer, E. Lizano, A.J. Houben, D. Bezdan, M. Báñez-Coronel, G. Kudla, E. Mateu-Huertas, B. Kagerbauer, J. González, K.C. Chen, E.M. Leproust, E. Martí, X. Estivill, Evidence for the biogenesis of more than 1,000 novel human microRNAs, Genome Biol. 15 (4) (2014) R57.
[18] X.M. Zhu, T. Han, I.L. Sargent, G.W. Yin, Y.Q. Yao, Differential expression profile of microRNAs in human placentas from preeclamptic pregnancies vs normal pregnancies, Am. J. Obstet. Gynecol. 200 (6) (2009) 661.e1–661.e7.
[19] J. Zhu, H. Fu, Y. Wu, X. Zheng, Function of lncRNAs and approaches to lncRNA-protein interactions, Sci. China Life Sci. 56 (10) (2013) 876–885.
[20] V.S. Akhade, D. Pal, C. Kanduri, Long noncoding RNA: Genome organization and mechanism of action, Adv. Exp. Med. Biol. 1008 (2017) 47–74.
[21] L. Deng, G. Li, R. Li, Q. Liu, Q. He, J. Zhang, Rho-kinase inhibitor, fasudil, suppresses glioblastoma cell line progression in vitro and in vivo, Cancer Biol. Ther. 9 (11) (2010) 875–884.
[22] K.R. Palmer, S. Tong, Kaitu'u-Lino TJ. Placental-specific sFLT-1: role in pre-eclamptic pathophysiology and its translational possibilities for clinical prediction and diagnosis, Mol. Hum. Reprod. 23 (2) (2017) 69–78.
[23] Y. Xu, Z. Ge, E. Zhang, Q. Zuo, S. Huang, N. Yang, D. Wu, Y. Zhang, Y. Chen, H. Xu, H. Huang, Z. Jiang, L. Sun, The lncRNA TUG1 modulates proliferation in trophoblast cells via epigenetic suppression of RND3, Cell Death Dis. 8 (10) (2017) e3104.
[24] C. Cao, J. Li, J. Li, L. Liu, X. Cheng, R. Jia, Long non-coding RNA Uc.187 is upregulated in preeclampsia and modulates proliferation, apoptosis, and invasion of HTR-8/SVneo trophoblast cells, J. Cell. Biochem. 118 (6) (2017) 1462–1470.
[25] L. Wu, W.Y. Song, Y. Xie, L.L. Hu, X.M. Hou, R. Wang, Y. Gao, J.N. Zhang, L. Zhang, W.W. Li, C. Zhu, Z.Y. Gao, Y.P. Sun, miR-181a-5p suppresses invasion and migration of HTR-8/SVneo cells by directly targeting IGF2BP2, Cell Death Dis. 9 (2) (2018) 16.
[26] B.Y. Mo, X.H. Guo, M.R. Yang, F. Liu, X. Bi, Y. Liu, L.K. Fang, X.Q. Luo, J. Wang, J.A. Bellanti, Y.F. Pan, S.G. Zheng, Long non-coding RNA GAPLINC promotes tumor-like biologic behaviors of fibroblast-like synoviocytes as MicroRNA sponging in rheumatoid arthritis patients, Front Immunol. 9 (2018) 702.
[27] Y.F. Lu, X.L. Cai, Z.Z. Li, J. Lv, Y.A. Xiang, J.J. Chen, W.J. Chen, W.Y. Sun, X.M. Liu, J.B. Chen, LncRNA SNHG16 functions as an oncogene by sponging MiR-4518 and up-regulating PRMT5 expression in glioma, Cell. Physiol. Biochem. 45 (5) (2018) 1975–1985.
[28] H.C. Lee, S.H. Jung, H.J. Hwang, et al., WIG1 is crucial for AGO2-mediated ACOT7 mRNA silencing via miRNA-dependent and -independent mechanisms, Nucleic Acids Res. 45 (11) (2017) 6894–6910.
[29] G. Song, R. Wang, J. Guo, X. Liu, F. Wang, Y. Qi, H. Wan, M. Liu, X. Li, H. Tang, miR-346 and miR-138 competitively regulate hTERT in GRSF1- and AGO2-dependent manners, respectively. Sci Rep. 5 (2015) 15793.
[30] H.E. Ritchie, D.J. Oakes, D. Kennedy, J.W. Polson, Early gestational hypoxia and adverse developmental outcomes, Birth Defects Res. 109 (17) (2017) 1358–1376.
[31] Y. Zhang, M. Fei, G. Xue, Q. Zhou, Y. Jia, L. Li, H. Xin, S. Sun, Elevated levels of hypoxia-inducible microRNA-210 in pre-eclampsia: new insights into molecular mechanisms for the disease, J. Cell. Mol. Med. 16 (2) (2012) 249–259.
[32] R. Luo, Y. Wang, P. Xu, G. Cao, Y. Zhao, X. Shao, Y.X. Li, C. Chang, C. Peng, Y.L. Wang, Hypoxia-inducible miR-210 contributes to preeclampsia via targeting thrombospondin type I domain containing 7A, Sci Rep. 6 (2016) 19588.
[33] M. Fang, H. Du, B. Han, G. Xia, X. Shi, F. Zhang, Q. Fu, T. Zhang, Hypoxia-inducible microRNA-218 inhibits trophoblast invasion by targeting LASP1: Implications for preeclampsia development, Int. J. Biochem. Cell Biol. 87 (2017) 95–103.
[34] C.L. Depoix, I. de Selliers, C. Hubinont, F. Debieve, HIF1A and EPAS1 potentiate hypoxia-induced upregulation of inhibin alpha chain expression in human term cytotrophoblasts in vitro, Mol. Hum. Reprod. 23 (3) (2017) 199–209.
[35] L. Guan, D. Ji, N. Liang, S. Li, B. Sun, Up-regulation of miR-10b-3p promotes the progression of hepatocellular carcinoma cells via targeting CMTM5, J. Cell. Mol. Med. 22 (7) (2018) 3434–3441.

[36] Y. Zhou, J. Huang, X. Yu, X. Jiang, Y. Shi, Y. Weng, Y. Kuai, L. Lei, G. Ren, X. Feng, G. Zhong, Q. Liu, H. Pan, X. Zhang, R. Zhou, C. Lu, LITAF is a potential tumor suppressor in pancreatic cancer, Oncotarget 9 (3) (2017) 3131–3142.
[37] Y. Shi, Y. Kuai, L. Lei, Y. Weng, F. Berberich-Siebelt, X. Zhang, J. Wang, Y. Zhou, X. Jiang, G. Ren, H. Pan, Z. Mao, R. Zhou, The feedback loop of LITAF and BCL6 is involved in regulating apoptosis in B cell non-Hodgkin's-lymphoma, Oncotarget 7 (47) (2016) 77444–77456.
[38] J. Zhou, Z. Yang, T. Tsuji, J. Gong, J. Xie, C. Chen, W. Li, S. Amar, Z. Luo, LITAF and TNFSF15, two downstream targets of AMPK, exert inhibitory effects on tumor growth, Oncogene 30 (16) (2011) 1892–1900.
[39] H.D. Major, R.A. Campbell, R.M. Silver, D.W. Branch, A.S. Weyrich, Synthesis of sFlt-1 by platelet-monocyte aggregates contributes to the pathogenesis of pre-eclampsia, Am. J. Obstet. Gynecol. 210 (6) (2014) 547.e1–547.e7.
[40] T.J. Kaitu'u-Lino, F.C. Brownfoot, S. Beard, P. Cannon, R. Hastie, T.V. Nguyen, N.K. Binder, S. Tong, N.J. Hannan, Combining metformin and esomeprazole is additive in reducing sFlt-1 secretion and decreasing endothelial dysfunction - implications for treating preeclampsia, PLoS One 13 (2) (2018) e0188845.
[41] L.C. Sánchez-Aranguren, C.T. Espinosa-González, L.M. González-Ortiz, S.M. Sanabria-Barrera, C.E. Riaño-Medina, A.F. Nuñez, A. Ahmed, J. Vasquez-Vivar, M. López, Soluble fms-like tyrosine kinase-1 alters cellular metabolism and mitochondrial bioenergetics in preeclampsia, Front. Physiol. 9 (2018) 83.